2021

Water Clarity at the River-Estuary Transition Zone: A Comparative Study of the James, Mattaponi, and Pamunkey Sub-estuaries

Rachel Henderson

Water Clarity at the River-Estuary Transition Zone: A Comparative Study of the James, Mattaponi, and Pamunkey Sub-estuaries

A thesis submitted in partial fulfillment of the requirements for the degree of Master of Science in Environmental Studies at Virginia Commonwealth University

by

Rachel Henderson
B.S. Biochemistry, Virginia Tech (2012)
M.S. Pharmaceutical Science, University of North Carolina at Chapel Hill (2014)

Thesis Advisor: Paul Bukaveckas Ph.D., Professor, VCU Center for Environmental Studies

Virginia Commonwealth University
Richmond, Virginia
January, 2021

Acknowledgment

I would like to thank my advisor, Dr. Paul Bukaveckas, for giving me the opportunity to do my research and providing invaluable guidance and support. I will undoubtedly continue to benefit from the tremendous amount of knowledge he has shared with me throughout this process. My sincere thanks to my committee members, Dr. Rima Franklin and Dr. James Vonesh, for providing insight and advice that helped me achieve this accomplishment. Last but not least, I would like to thank my family and fiancé for their continuous love and support. I am incredibly grateful to have them in my life.

Table of Contents

Abstract

Water clarity is a key parameter for monitoring water quality and often used to assess habitat suitability for submerged aquatic vegetation (SAV). Light attenuation, a measure of water clarity, is impacted by colored dissolved organic matter (CDOM), and by suspended particulates which include living and non-living components. We anticipated that the relative importance of these factors in regulating light attenuation would vary among the upper portions of three sub-estuaries differing in morphometry, hydrology, and degree of human influence. The James is characterized by eutrophic conditions and high algal abundance, whereas the Mattaponi and Pamunkey exhibit lower phytoplankton production. The Mattaponi and Pamunkey have extensive floodplains, which likely serve as sources for CDOM. We measured light attenuation, turbidity, total suspended solids (TSS), chlorophyll a (CHLa), dissolved organic carbon (DOC), and CDOM over a 3-year period at sites within each estuary. These parameters, along with discharge, were analyzed to identify factors regulating light attenuation. The Mattaponi and Pamunkey exhibited greater light attenuation than the James. Turbidity and TSS were the strongest predictors of variation in light attenuation at all sites. CHLa was not found to be a significant predictor of light attenuation at any of the sites. Light scattering per unit of suspended particle mass was twice as high in the James compared to the other rivers despite similarities in suspended particle size and mass. Linear statistical models based on suspended solids and dissolved organic matter accounted for 64-93% of the range of variation in light attenuation. Understanding factors that regulate light attenuation is important when considering management activities intended to improve estuarine water clarity and SAV habitat.

Introduction

The depth to which sunlight is able to penetrate the water column is an important indicator of water clarity in estuarine systems. Reductions in light availability limit photosynthesis by phytoplankton and benthic plants thereby affecting multiple ecological processes including hypoxia, nutrient cycling, sediment trapping, and wildlife predation behavior (Davies-Colley et al. 2014; Abdelrhman 2017). Adequate water clarity is especially important to primary productivity in the Chesapeake Bay and its tributaries where shallow areas (< 2 m) have historically supported diverse communities of submerged aquatic vegetation (SAV) (Kemp et al. 2005). SAV serve critical functions in aquatic environments by absorbing excess nutrients, preventing shoreline erosion, and supporting wildlife as a source of food and habitat (Dennison et al. 1993). Since 1960, reductions in light availability and water clarity have caused SAV acreage to decrease dramatically in the Bay (Kemp et al. 2005; Baldizar and Rybicki 2006). Multiple agencies are working to develop and implement management strategies aimed at achieving minimal light requirements for SAV survival.

Underwater light sensors are used to measure photosynthetically active radiation (PAR) within the water column. Light attenuation is represented by the diffuse attenuation coefficient (K_d), which is calculated from the decline in down-welling irradiance with depth (Kirk 2011). Smaller attenuation coefficient values are indicative of greater water clarity. As depth increases, underwater irradiance is diminished through absorption and/or scattering by dissolved organic carbon (DOC) and suspended particulate matter (Kirk 1994; Gallegos 1994; Gallegos and Moore 2000). Colored dissolved organic matter (CDOM) is the fraction of DOC that contributes to light attenuation. It is leached into the water column from decaying plant material. Suspended particulate matter is composed of non-living suspended solids (e.g., clay, silt, and sand) as well as living cells (e.g., phytoplankton and bacteria). Light attenuation per unit mass of suspended particulate matter is controlled by the size, shape, and composition of particles. For example, light attenuation by spherical quartz particles peaks at a particle diameter of 1.2 μm and then declines with increasing diameter (Davies-Colley et al. 2014). For organic particles, this peak occurs at around 5 μm, the size of many forms of phytoplankton (Davies-Colley and Smith 2001). In general, finer sediments attenuate light more strongly and have a greater negative impact on water clarity than larger particles. Two analytical methods commonly used to measure

suspended solids are total suspended solids (TSS) and turbidity. TSS is a measure of the mass concentration of suspended solids per a given volume, whereas turbidity is a measure of light scattering caused by suspended solids. Since TSS measurements do not provide information on particle size (and therefore light scattering properties), TSS may not correlate as well with measurements of water clarity when compared to turbidity.

Quantifying impacts from various light attenuating factors can be challenging due to their variable contributions to water clarity under changing conditions (e.g., storm events and algal blooms). This is especially true in estuarine environments where the confluence of river water and sea water results in a diverse collection of optically active constituents from both terrestrial and aquatic sources (Xu et al. 2005). Although non-linearity is often present in estuarine water quality data, linear expressions are often used for light attenuation modeling (Gallegos and Moore 2000). Multiple linear regression (MLR) models have been used to partition sources of water column light attenuation in estuaries (Xu et al. 2005; Baldizar and Rybicki 2006; Chen and Doering 2016). For example, the below MLR equation assumes that contributions of DOC, TSS, and phytoplankton, indexed by chlorophyll a (CHLa), to light attenuation (K_d) are proportional to their concentrations in the water column and are additive in nature.

$$K_d = K_w + k_{om[DOC]} + k_{s[TSS]} + k_{c[CHLa]}$$

In this example, K_w is the partial attenuation coefficient due to water itself, and k_{om}, k_s, and k_c are the specific-attenuation coefficients due to DOC, TSS, and CHLa, respectively. Parameterization of these models provides a basis for estimating light attenuation from constituent components and to quantify their relative importance to water clarity.

Contributions from light attenuating factors vary depending on environmental conditions within a waterbody. For example, CDOM concentrations are known to vary considerably throughout estuaries, typically with higher concentrations near freshwater or wetland sources and lower concentrations in more oceanic waters (Rochelle-Newall and Fisher 2002). Therefore, CDOM contributions to K_d may be less significant in more saline areas compared to freshwater areas. Water clarity can also fluctuate over the course of a year owing to seasonal factors such as variation in river discharge and the occurrence of algal blooms. Following increases in river

discharge, water clarity may be reduced by suspended solids due to elevated loads from catchments. In eutrophic waters, high densities of phytoplankton may be the dominating factor affecting water clarity. Previous studies in estuarine waters of the Chesapeake Bay and Narragansett Bay found that TSS dominated variability of K_d (Gallegos 2001; Gallegos et al. 2005; Abdelrhman 2017). In a Florida estuary, CDOM and turbidity accounted for the greatest amount of variation in light attenuation, while CHLa accounted for significantly less (Chen and Doering 2016). Our knowledge of inter-estuarine differences in the factors regulating water clarity is largely based on studies conducted in the lower, saline portions of the estuary. Less is known regarding the factors regulating water clarity in the upper, tidal fresh segments of these estuaries.

The objectives of this study were to evaluate the contributions of various constituents on water clarity, and to examine how relative contributions to light attenuation vary among the upper portions of three sub-estuaries of the Chesapeake Bay. The estuaries differ in their morphometry, hydrology, and degree of human influence. Information from this study may lead to a better understanding of the factors regulating light attenuation in the upper estuary and aid management actions to restore water clarity. In addition to assessing impacts of light attenuating factors on water clarity, we aimed to answer the following questions:

- How does light attenuation vary seasonally?
- Are there long-term trends in light attenuation?
- Is water clarity controlled by suspended particle size?
- Is light attenuation influenced by variations in discharge and salinity?
- Do relationships between water clarity and light attenuating constituents follow nonlinear trends?
- Do site habitats meet water quality standards for SAV survival?

Methods

Study Sites

The James, Pamunkey and Mattaponi estuaries are the most southern tributaries of Chesapeake Bay. Land use in the James River watershed is predominately forest (71%) and agriculture (23%) but also includes a large metropolitan area (Richmond, VA) located at the Fall Line (Smock 2005). The Pamunkey and Mattaponi sub-estuaries together form the York River Estuary (YRE), which has similar proportions of forested (61%) and agricultural (21%) lands, but without a major urban center (Reay 2009). The estuaries are divided into segments based on salinity: tidal fresh (TF, < 0.5 ppt), oligohaline (OH, 0.5–5 ppt), mesohaline (MH, 5–18 ppt), and polyhaline (PH, > 18 ppt). This study focuses on the upper reaches of each estuary which encompass the upper and lower TF segments of the James (JMS UTF, JMS LTF), OH segments of the Pamunkey (PMK OH) and Mattaponi (MPN OH), and the MH segment of the York (York MH; *Fig. 1*).
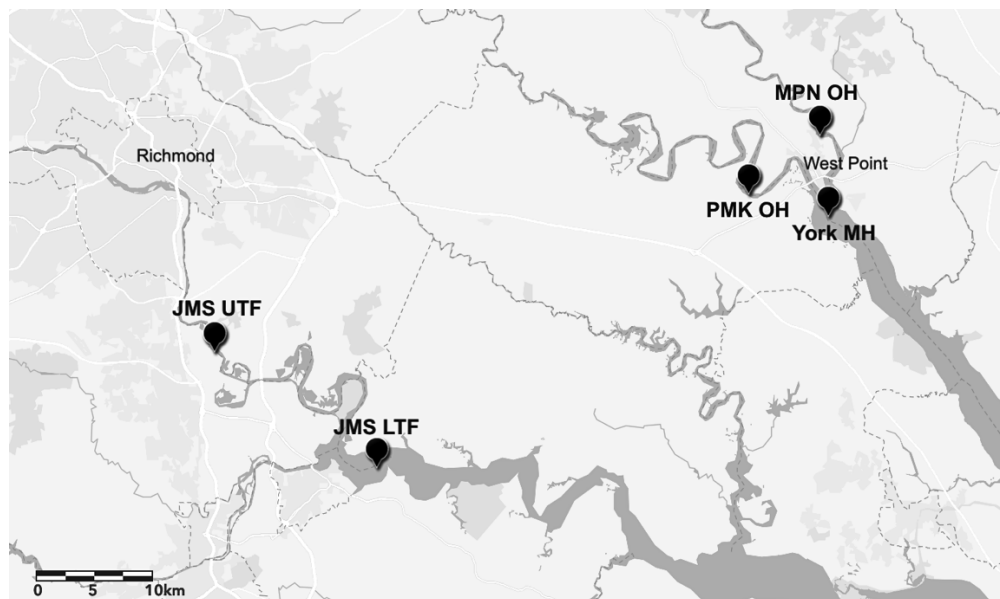
Fig. 1: Map of site locations in the James River upper (JMS UTF) and lower (JMS LTF) tidal fresh segments, Mattaponi (MPN OH) and Pamunkey (PMK OH) oligohaline segments, and the York mesohaline (YRK MH) segment.

In the James River Estuary (JRE), strong tidal forces create a well-mixed system both vertically and laterally. The freshwater replacement times in the TF segment range from < 4 days during colder months to > 50 days in warmer months due to seasonal variability in runoff from the catchment (Bukaveckas et al. 2018). The TF region of the James River extends from the Fall Line at Richmond, VA to the confluence with the Chickahominy River, a length of 115 km. This region of the estuary is further divided into upper and lower segments. Compared to the narrow riverine morphometry of the upper TF segment, the lower segment is characterized by a more estuarine morphometry with a broad channel (Bukaveckas, et al. 2011; Wood and Bukaveckas 2014). Mean channel depths in the upper and lower TF are 2.7 and 2.5 m, respectively (Tassone and Bukaveckas 2019). The JRE is a highly productive waterbody that receives elevated loads of suspended sediments and nutrients from its large catchment and nearby metropolitan discharges (Bukaveckas and Isenberg 2013). The JMS LTF site is located within the TF CHLa maximum (Bukaveckas et al. 2011). Elevated phytoplankton growth in this area is attributed to favorable light and nutrient conditions and longer water residence times (Qin and Shen 2017). Previous studies have shown that the TF segment retains a large fraction of particulate matter (Bukaveckas et al. 2018; Bukaveckas and Isenberg 2013) resulting in high proportions of suspended particulate matter originating from terrestrial origins, despite elevated levels of autochthonous production (Wood 2016). TSS in this segment has been found to be positively correlated with discharge, but does not exhibit a consistent seasonal pattern (Bukaveckas et al. 2019).

The YRE is a brackish, partially mixed, coastal plain tributary that receives freshwater inputs from the Pamunkey and Mattaponi. The York is relatively wide and straight compared to the Mattaponi and Pamunkey, which have strongly meandering channels that are deeper at the bends (~15 m) and shallow in the stretches (~5 m). The Mattaponi and Pamunkey are comprised of TF and OH segments, whereas the York is MH. The YRE varies between stratified and well-mixed conditions depending on tidal cycles (Haas 1977; Hayward et al. 1982). Mixing of the water column can supply regenerated nutrients to the surface water, stimulating phytoplankton production (Haas et al. 1981). Terrestrial sources dominate riverine sediment inputs; tidal and nearshore erosion are also a significant source of suspended sediment (Reay 2009). The York MH site is located within the estuary turbidity maximum (ETM) where suspended sediments occur at greater concentrations than observed either upriver or seaward. ETMs can shift

seasonally, migrating upriver during periods of low freshwater discharge (Reay 2009). The Mattaponi and Pamunkey Rivers receive significant wetland drainage delivering substantial amounts of dissolved organic matter (DOM; Lake et al. 2013).

Sample Collection and Analysis

Light attenuation and associated variables (TSS, turbidity, particle density and size, CDOM, DOC and CHLa) were measured at five sites within the James (UTF, LTF), Mattaponi (OH), Pamunkey (OH), and York (MH) estuaries. K_d measurements and water samples were collected on ~65 sampling dates at each site at 1- to 2-week intervals from June 2017 through October 2019 (weekly in 2017 and bi-weekly in 2018 and 2019). During each sampling event, water quality parameters (e.g., temperature and specific conductivity) were measured in the field using a YSI Pro DSS sonde. Irradiance (PAR) was measured with a LI-COR model LI-1400 data logger equipped with underwater and surface quantum sensors (LI-192SA and LI-190SA, respectively). Underwater irradiance measurements consisted of vertical profiles from 0.01 m to 2 m at 0.5-m intervals with two or more replicate profiles obtained at each sampling. Light attenuation coefficients (K_d; m^{-1}) were derived from a linear regression of the down-welling irradiance versus depth (Kirk 1994). Water samples were obtained near the surface (< 1 m) and analyzed for suspended particulate (TSS, CHLa) and dissolved organic fractions (CDOM, DOC). DOC was analyzed less frequently than other parameters and at somewhat irregular intervals. CDOM sampling did not begin until October 2018 and was not collected at the JMS UTF site. Samples for Coulter counter analysis (particle density and size) were collected from April 2019 through October 2019 at all sites except the York MH.

Analysis of water samples followed protocols developed for the VCU Environmental Analysis Lab, a state-accredited water quality testing facility. Turbidity was measured with a HACH model 2100 Turbidimeter. CHLa samples were filtered thru Whatman GF/A glass filters (0.5 μm), extracted for 18 h in buffered acetone and analyzed on a Turner Design TD-700 Fluorometer. TSS was determined gravimetrically using pre-weighed, pre-combusted Whatman GF/A glass filters (0.5 μm). DOC was measured by persulphate digestion followed by infrared detection using a Schimadzu TOC analyzer. CDOM samples were filtered through Whatman GF/A glass (0.5 μm) and analyzed at a wavelength of 440 nm using a Schimadzu UV-1800 (5

cm pathlength) dual-beam spectrophotometer. Particle-size samples were preserved with Lugol's iodine solution (4 drops into 40 mL sample) and refrigerated until analysis. Samples were analyzed using a Beckman Coulter Multisizer 4 Coulter Counter fitted with a 100-μm aperture tube. The operational range in particle size measurements was between 2 μm and 60 μm. The instrument measures all particles inclusive of cells (bacteria, phytoplankton) and non-living particulates (e.g., silt and clay). Samples were diluted with electrolyte solution for a range of concentrations (2x, 4x, 8x, 16x). The 2x dilution typically exceeded the instruments particle count limit (113,000), and therefore most samples were measured in triplicate at 4x, 8x, and 16x. Results were reported as particle density (#/mL) and particle size (μm) and were corrected for dilution accordingly. Mean particle mass (ng) was calculated by dividing TSS by particle density.

Data Sources

Discharge data measured at upriver USGS stations were included in this analysis as concentrations of particulate matter in the estuary may vary with changes in flow. Daily mean discharge data were obtained from USGS gauge stations on the James (at Richmond; #02037500), Appomattox (at Matoaca; #02041650), Mattaponi (near Beulahville; # 01674500), and Pamunkey Rivers (near Hanover; #01673000). Daily discharges for the JMS LTF site were calculated by combining daily values from the Richmond and Appomattox stations. Daily discharges for the York MH site were calculated by combining discharge values from the Mattaponi and Pamunkey stations. The 7-day mean discharge preceding each sampling event was used in the data analysis.

In addition to the sampling conducted for this study, we analyzed long-term data (1994-2019) from the Chesapeake Bay Program (obtained from CBP DataHub) which included monthly monitoring of K_d in the James, Pamunkey, and York Rivers. Stations used in this study were selected based on location and available data. Two CBP sites (TF5.5 and RET4.3) were in the same locations as our study sites (JMS LTF and York MH, respectively). We also selected a station in the TF segment of the Pamunkey (TF4.2), which was in proximity to our Pamunkey OH site. At each station, underwater light intensity was measured at depth intervals of either 0.25

or 0.5 m. Each station was visited on average 8 times a year at somewhat irregular intervals. Ancillary data for these sites included turbidity, TSS, CHLa, and DOC.

Continuous monitoring data (PAR, turbidity) were obtained from the VCU Rice Center Research Pier (2014–2019) located ~2 km downriver from the JMS LTF site. PAR and turbidity measurements were recorded year-round and used to estimate daily underwater irradiance. Turbidity data was collected using a YSI 6600 water quality sonde (2014) or YSI EXO2 water quality sonde (2015–2019). Sondes were calibrated every 3 weeks. PAR data were collected using a LI-COR surface quantum sensor (LI-190SA). The 15-min PAR measurements were converted to total daily PAR values. Average daily underwater irradiance in the water column (I_{wc}; E m^{-2} day^{-1}) was calculated taking into account the average (cross-sectional) depth of the channel using the following equation (Gosselain et al. 1994):

$$I_{wc} = I_s/(K_d \text{ x } Z_{x\text{-sec}})$$

Where I_s is daily incident solar radiation (E m^{-2} day^{-1}), represented by total daily Rice Rivers Center Research Pier PAR. K_d (m^{-1}) is specific light attenuation coefficient, and $Z_{x\text{-sec}}$ is cross-sectional average depth of the channel (2.5 m in the James lower TF).

Data Analysis

Statistical analyses were performed using RStudio statistical software. Regressions and ANOVAs were performed using the "base" R package. Separate one-way ANOVAs were used to test for differences in K_d data and particle size data among study sites. Linear regression models were used to examine relationships between K_d and each of the predictor variables (turbidity, TSS, CHLa, DOC, CDOM, and discharge). Linear regression models were also used to examine relationships between independent variables (turbidity vs TSS, turbidity vs particle data, CDOM vs DOC, CDOM vs specific conductivity, turbidity vs discharge, CDOM vs discharge). MLR models were used to assess the relative importance of three parameters in influencing light attenuation: suspended solids (TSS or turbidity), algae (CHLa), and DOM (CDOM or DOC). Each model tested incorporated all three parameters. Top performing models at each site were identified by the greatest R^2 value. The JMS UTF site was excluded from models including CDOM since these data were not collected at this site. To determine the

contribution from predictor variables (turbidity, CHLa, DOC or CDOM) to K_d, we multiplied the mean concentration of each variable over the study period by its regression coefficient.

Generalized additive models (GAMs) were performed using the "mgcv" package in RStudio. These models are recommended for data that follow non-linear trends. Since water quality data are often not normally distributed, the use of non-parametric techniques is advantageous. Long-term data (1994-2019) obtained from the CBP DataHub was used in GAM models to analyze K_d against decimal date (to assess long term-trends) and day of year (to describe seasonal patterns). GAMs were also used to analyze data collected as part of this study to assess non-linearity in statistical relationships between K_d and each of the predictor variables (TSS or turbidity, CHLa, and DOC or CDOM). The package default thin plate regression spline was used for GAM analyses. A cyclic cubic regression spline was used to depict seasonal effects. Model results were scaled to center on mean K_d to assess the effect of each predictor variable. An additional GAM model ($R^2 = 0.50$) was derived to predict daily K_d in the James lower TF. JMS LTF K_d was used as the response variable and turbidity ($p < 0.001$) measured at the Rice Rivers Center Research Pier on corresponding sampling dates was used as a predictor variable along with day of year ($p = 0.017$) and decimal date ($p = 0.124$). Average daily K_d from 2014-2019 was predicted using daily turbidity measurements at the Rice Rivers Center Research Pier. Average daily underwater irradiance (I_{wc}; E m^{-2} day^{-1}) was calculated in the James lower TF using Rice Rivers Center Research Pier PAR and GAM predicted K_d. The average underwater irradiance was indexed into spring (day of year 81-172) and summer (day of year 173-266) datasets and used to characterize inter-annual variation in seasonal light availability from 2014-2019.

Results

Variation in Light Attenuation and Predictor Variables

Average light attenuation among the 5 sites ranged from 1.85 ± 0.15 m^{-1} (JMS UTF) to 3.23 ± 0.11 m^{-1} (PMK OH; *Fig. 2*). Corresponding photic depths (depth of 1% light penetration) were 2.49 m (JMS UTF) and 1.42 m (PMK OH). Differences in light attenuation among sites

were statistically significant ($p < 0.001$). A further analysis using Tukey's HSD test revealed that the JMS UTF site had the greatest water clarity, followed by the JMS LTF and York MH sites, and the MPN and PMK OH sites. Overall, inter-site differences in light attenuation generally tracked patterns in turbidity, TSS, and DOC. Mean TSS concentrations were higher among the MPN OH, PMK OH and York MH sites (30.5 to 32.7 mg L^{-1}) compared to the JMS sites (13.8 to 18.8 mg L^{-1}). The PMK OH, MPN OH and York MH sites also exhibited higher turbidity (20.4 to 26.2 NTU) relative to the JMS sites (16.0 to 18.9 NTU). DOC concentrations were higher among the MPN OH, PMK OH and York MH sites (6.4 to 6.8 mg L^{-1}) relative to the JMS sites (3.7 to 4.8 mg L^{-1}), whereas CDOM did not exhibit consistent differences among the drainages with highest values at MPN OH (3.13 m^{-1}) and lowest values at the York MH (1.84 m^{-1}). The JMS LTF site had the highest mean CHLa concentration (27.7 µg L^{-1}), while the JMS UTF had the lowest (4.2 µg L^{-1}).
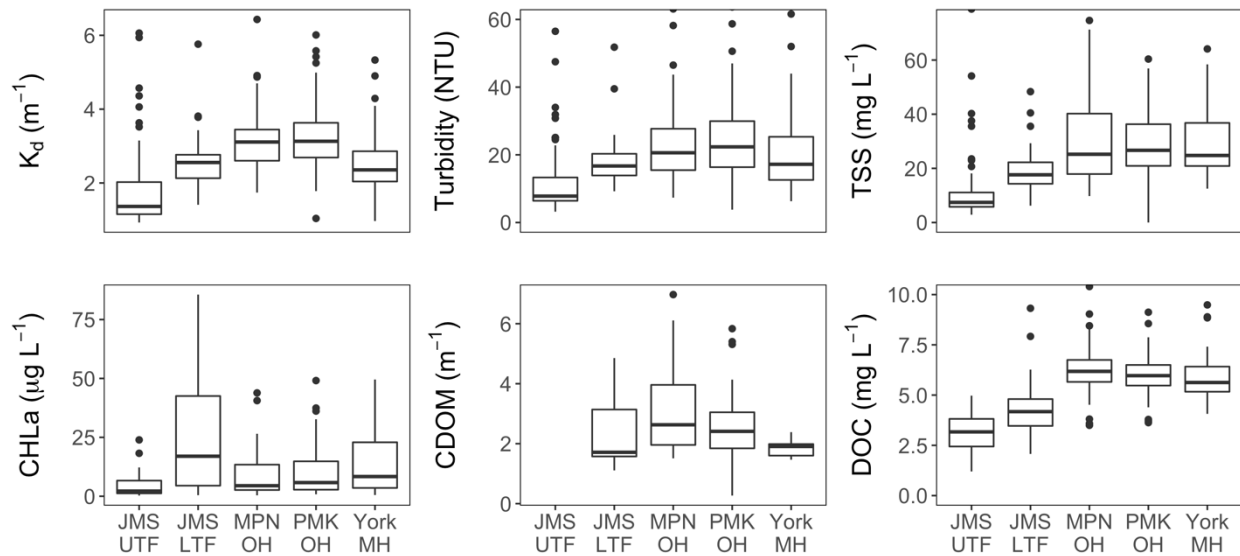

Fig. 2: Boxplots showing variation in light attenuation (K_d), turbidity, TSS, CHLa, CDOM and DOC among stations located in the James River upper (JMS UTF) and lower (JMS LTF) tidal fresh segments, Mattaponi (MPN OH) and Pamunkey (PMK OH) oligohaline segments, and the York mesohaline (York MH) segment. Y-axis scales were truncated causing some outliers to be excluded from plots. The number of excluded outliers are as follows: turbidity = 8, TSS = 8, DOC = 12.

Seasonal and Inter-annual Trends

Patterns in K_d were relatively similar among sites with considerable variation throughout the year and no obvious seasonal trend (*Fig.* 3). Long-term data (1994-2019) collected by the Chesapeake Bay Program was used to identify annual and seasonal trends in K_d (*Fig. 4*). Both the Pamunkey and York sites showed significant seasonal declines in K_d in late summer to minimum values of ~2.5 m^{-1} following spring maxima of 3.5-4.0 m^{-1}. In contrast, seasonal patterns in the James lower TF showed minimum values in spring (~2.8 m^{-1}) and relatively similar values throughout the rest of the year (~3.5 m^{-1}). Significant long-term trends were observed in the York which showed a decline in light attenuation from ~3.6 m^{-1} to 2.8 m^{-1} over the 25-year span. A decreasing trend in light attenuation was also observed in the James, but was only marginally significant ($p = 0.054$). Overall, seasonal and long-term trends accounted for only a small proportion (5.5-17%) of the variation in K_d at each of the sites.
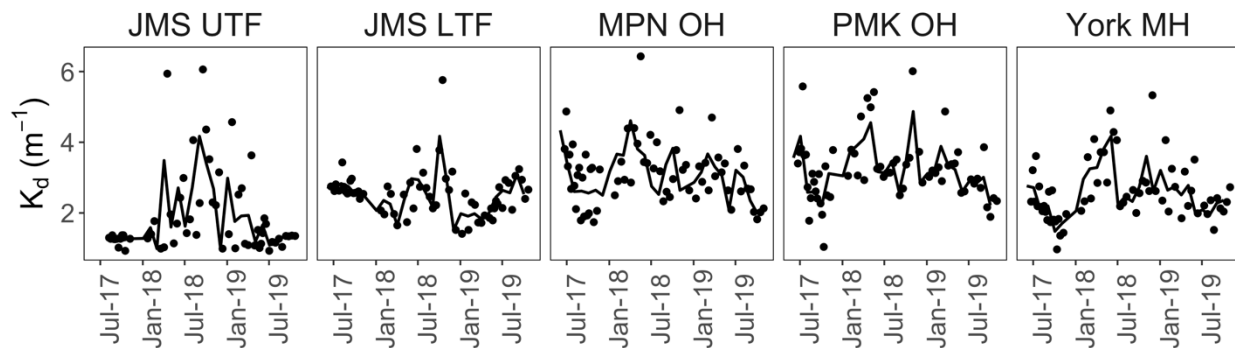

Fig. 3: Light attenuation at stations located in the James River upper (JMS UTF) and lower (JMS LTF) tidal fresh segments, Mattaponi (MPN OH) and Pamunkey (PMK OH) oligohaline segments, and the York mesohaline (York MH) segment. Solid points denote observed values and lines denote monthly averages.
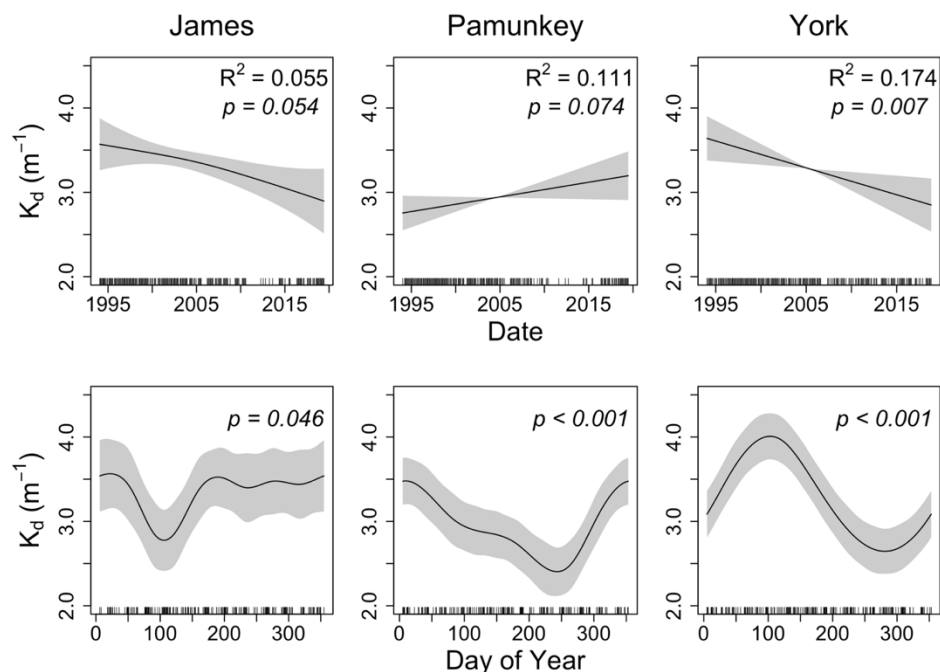
Fig. 4: Inter-annual (decimal date) and seasonal (day of year) variation in light attenuation in the James lower TF (CBP TF5.5), Pamunkey TF (CBP TF4.2), and York MH (CBP RET 4.3) segments derived from a GAM analysis of Chesapeake Bay Program data. Displayed R^2 is for the overall model. Gray shading represents confidence intervals.

Factors Contributing to Light Attenuation

Linear regression models were used to assess the influence of turbidity, TSS and CHLa on K_d at each site (*Fig. 5*). Turbidity and TSS were the strongest predictors of variation in K_d at all five sites. Turbidity was a stronger predictor of K_d at the JMS sites and York site ($R^2 = 0.63$ to 0.85) compared to the MPN and PMK OH sites ($R^2 = 0.44$ and 0.43, respectively). A comparison of regression slopes revealed differences among the sites in the rate of change in K_d as a function of turbidity. Highest slopes were observed among the York MH (0.061 ± 0.005 m^{-1} NTU^{-1}), JMS UTF (0.052 ± 0.003 m^{-1} NTU^{-1}) and JMS LTF (0.050 ± 0.005 m^{-1} NTU^{-1}) sites. Increases in light attenuation as a function of turbidity were lower at the MPN and PMK OH sites (0.036 ± 0.005 and 0.043 ± 0.006 m^{-1} NTU^{-1}, respectively). TSS was a strong predictor of K_d at the JMS UTF ($R^2 = 0.73$) and LTF ($R^2 = 0.62$) sites, and a weaker predictor of variation among the YRE sites ($R^2 = 0.20$ to 0.30). The JMS UTF and LTF also exhibited larger slopes

13

(0.054 ± 0.004 and 0.068 ± 0.007 m^{-1} mg^{-1} L, respectively) compared to the MPN OH, PMK OH and York MH sites (0.019 ± 0.004, 0.025 ± 0.006, and 0.026 ± 0.005 m^{-1} mg^{-1} L, respectively). CHLa was not found to be a significant predictor of light attenuation at any of the 5 sites. Slopes of linear regressions between turbidity (an optical property) and TSS (a gravimetric property) were analyzed to better understand the effects of suspended particulate matter on light scattering. We observed a strong positive relationship between turbidity and TSS at each site ($p < 0.001$). Comparisons between regression slopes revealed that the JMS UTF and LTF sites had almost double the amount of turbidity per unit of TSS (slopes = 1.03 ± 0.06 and 0.99 ± 0.13 NTU mg^{-1} L , respectively) compared to the MPN OH, PMK OH, and York MH sites (slopes = 0.54 ± 0.04, 0.45 ± 0.10, and 0.38 ± 0.07 NTU mg^{-1} L, respectively).

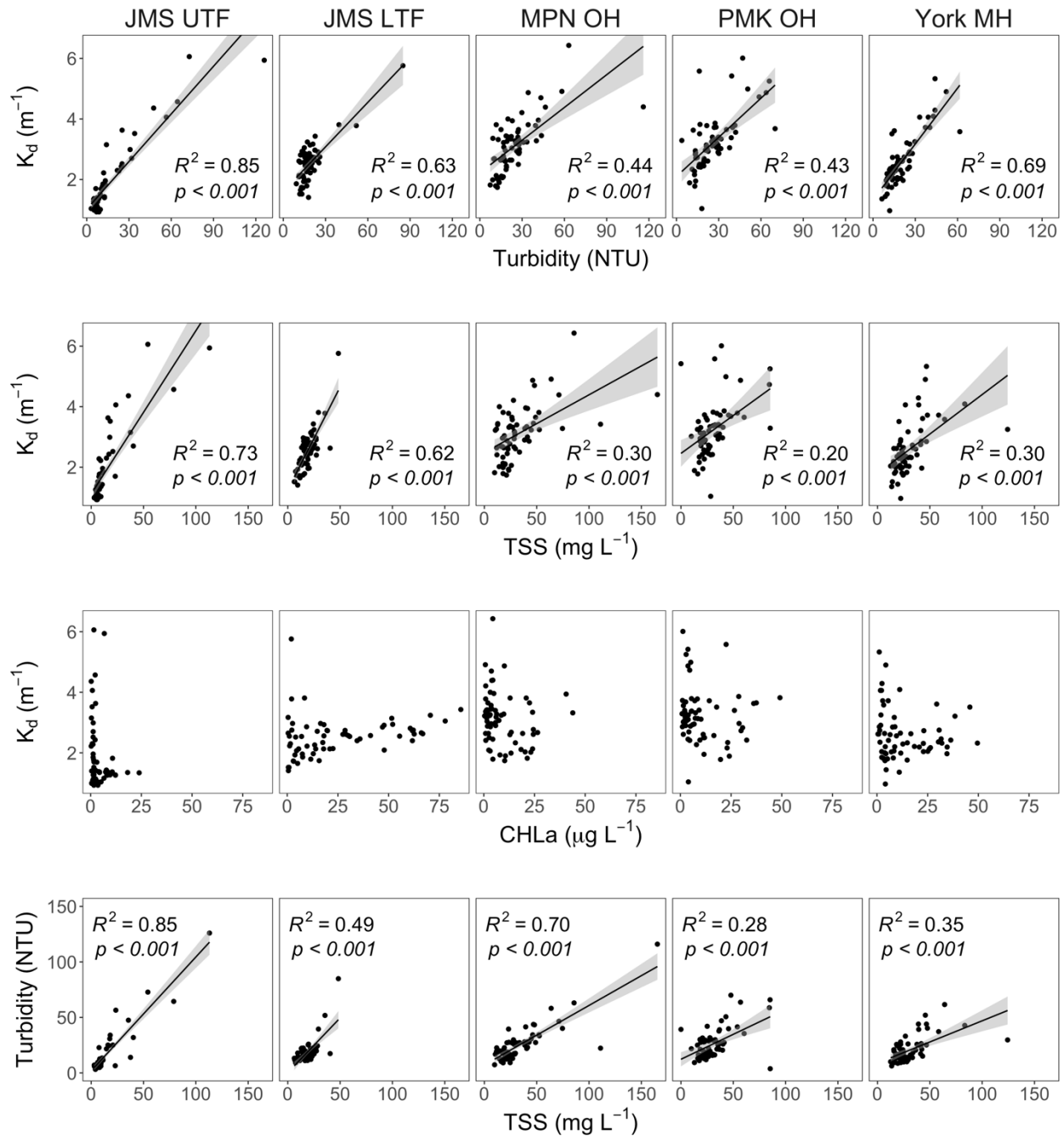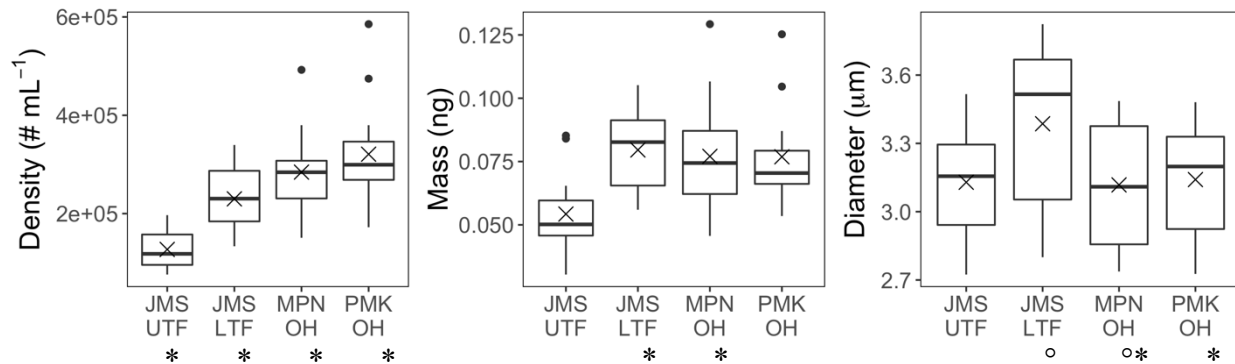*Fig. 5: Linear regressions of K_d vs turbidity, TSS, and CHLa, as well as, turbidity vs TSS at stations located in the James River upper (JMS UTF) and lower (JMS LTF) tidal fresh segments, Mattaponi (MPN OH) and Pamunkey (PMK OH) oligohaline segments, and the York mesohaline (York MH) segment. Models with statistically significant results (p < 0.05) display regression lines. Gray shading represents confidence intervals.*

To determine if particle characteristics influenced light attenuation, we compared differences in particle size and density among study sites (*Fig. 6*). Results from one-way ANOVAs showed that sites differed significantly in regards to particle density ($p < 0.001$), mass ($p = 0.007$), and diameter ($p = 0.048$). Particle density was lowest at the JMS UTF sites (127,000 ± 11,400 mL^{-1}) and highest at the PMK and MPN OH sites (321,000 ± 28,300 mL^{-1} and 284,000 ± 24,000 mL^{-1}, respectively). Particle mass was lowest at the JMS UTF site (0.054 ± 0.005 ng) and similar among the other 3 sites (0.077 to 0.080 ng). Particle diameter was greatest at the JMS LTF site (3.39 ± 0.10 μm) and similar among the other 3 sites (3.12 to 3.14 μm). Analysis of site-specific relationships showed that there was a significant positive association between turbidity and particle density at 3 of the 4 sites (excluding JMS UTF) (*Fig. 7*). There was no significant relationship between turbidity and particle mass and only marginally significant relationships with turbidity and particle diameter at MPN and PMK OH sites ($R^2 > 0.25$, $p > 0.05$).

Fig. 6: Variation in particle density, mass, and diameter among stations located in the James River upper (JMS UTF) and lower (JMS LTF) tidal fresh segments, and Mattaponi (MPN OH) and Pamunkey (PMK OH) oligohaline segments. "X" symbols represent mean values while solid points denote outliers. Matching symbols below site name indicate sites with significant similarities according to a Tukey's HSD test.
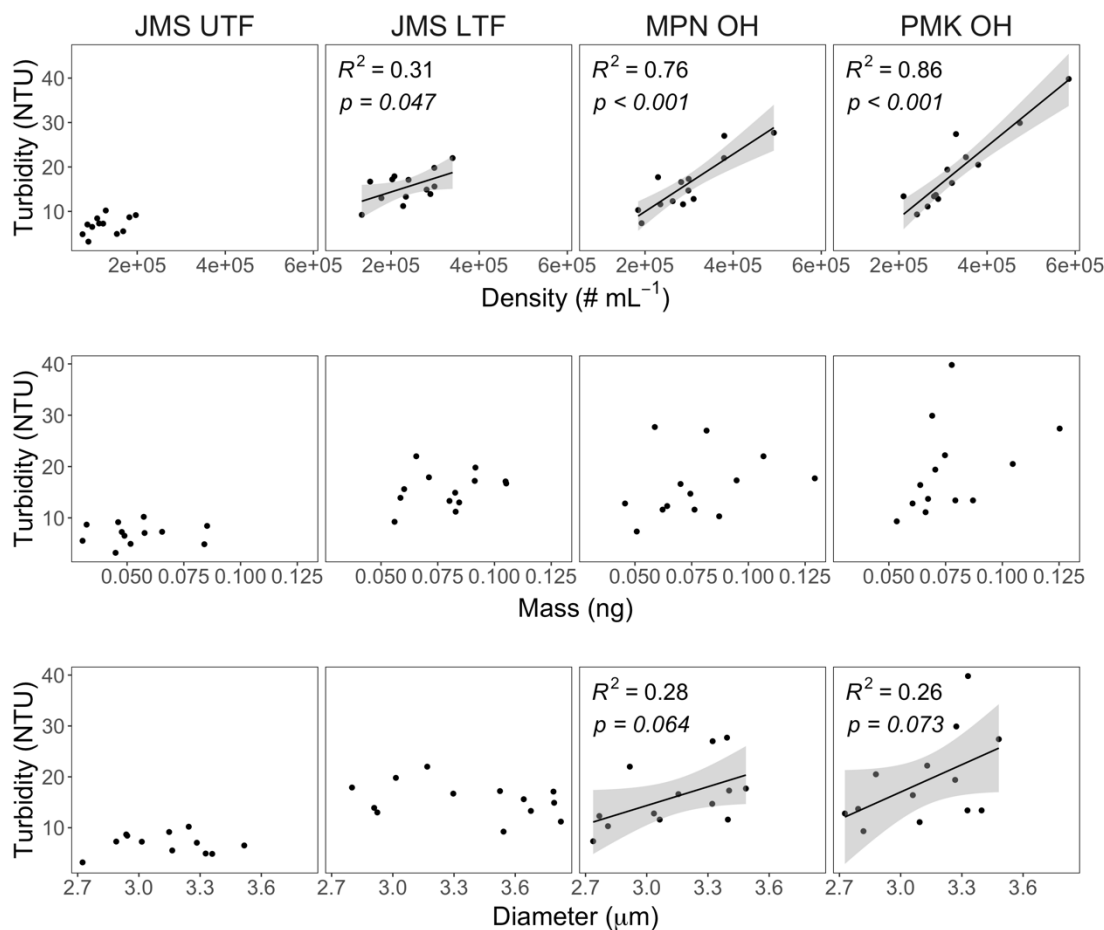
16

Fig. 7: Linear regressions of turbidity against particle density, mass, and diameter at stations located in the James River upper (JMS UTF) and lower (JMS LTF) tidal fresh segments and Mattaponi (MPN OH) and Pamunkey (PMK OH) oligohaline segments. Models with statistically significant (p < 0.05) and marginally significant (0.05 ≤ p < 0.10) results display regression lines. Gray shading represents confidence intervals.

Regression analyses revealed that CDOM was a significant predictor of light attenuation at the JMS LTF, MPN OH, and PMK OH sites (no data for JMS UTF; *Fig. 8*). The linear regressions accounted for ~30% of variation in K_d at all 3 sites. There was no significant relationship between CDOM and K_d at the York MH site. Comparisons of slope regressions revealed similar amounts of light attenuation per unit of CDOM across sites excluding the York MH site (0.269 ± 0.095 at JMS UTF to 0.366 ± 0.122 at PMK OH). Linear regressions of K_d against DOC did not show a significant relationship at any site. Additionally, CDOM and DOC did not show a high correlation.
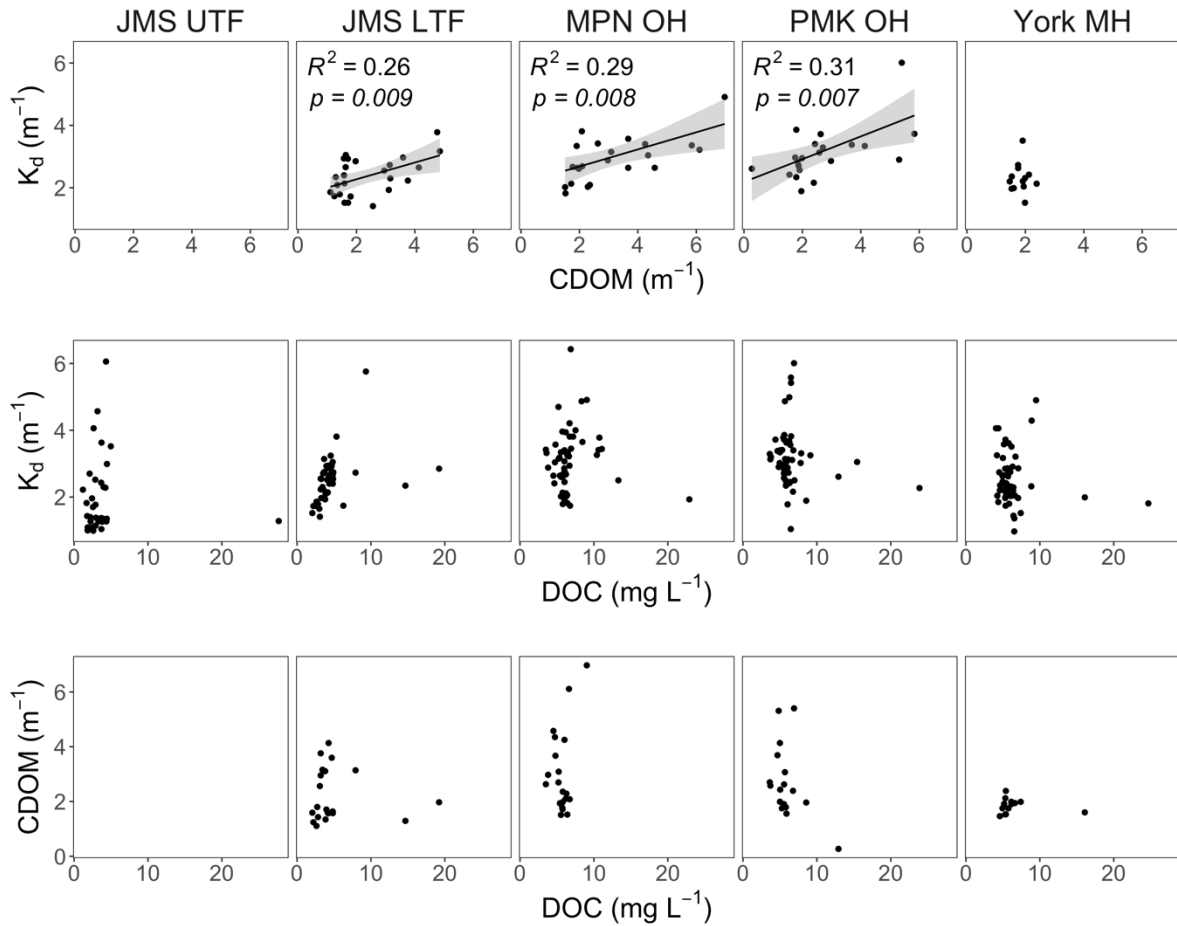
Fig. 8: Linear regressions of K_d vs CDOM and DOC and CDOM vs DOC at stations located in the James River upper (JMS UTF) and lower (JMS LTF) tidal fresh segments, Mattaponi (MPN OH) and Pamunkey (PMK OH) oligohaline segments, and the York mesohaline (York MH) segment (no CDOM for JMS UTF). Models with statistically significant results (p < 0.05) display regression lines. Gray shading represents confidence intervals.

Linear regressions revealed that discharge was a significant predictor of K_d at only two sites (JMS UTF and York MH) and accounted for a small proportion of the variation ($R^2 = 0.24$ and 0.32, respectively; *Fig. 9*). Discharge showed a moderately weak correlation with turbidity at the JMS LTF ($R^2 = 0.34$) and York MH ($R^2 = 0.35$) sites and a weak correlation at the JMS UTF site ($R^2 = 0.14$). CDOM concentrations were strongly and positively correlated with discharge at 3 of the 4 sites ($R^2 > 0.50$, $p < 0.001$). At the same 3 sites, CDOM concentrations showed negative correlations with increases in specific conductivity, a surrogate for salinity (JMS LTF $R^2 = 0.18$, MPN OH $R^2 = 0.52$, PMK OH $R^2 = 0.37$). At the York MH site, CDOM was negatively correlated with discharge and positively correlated with specific conductivity.
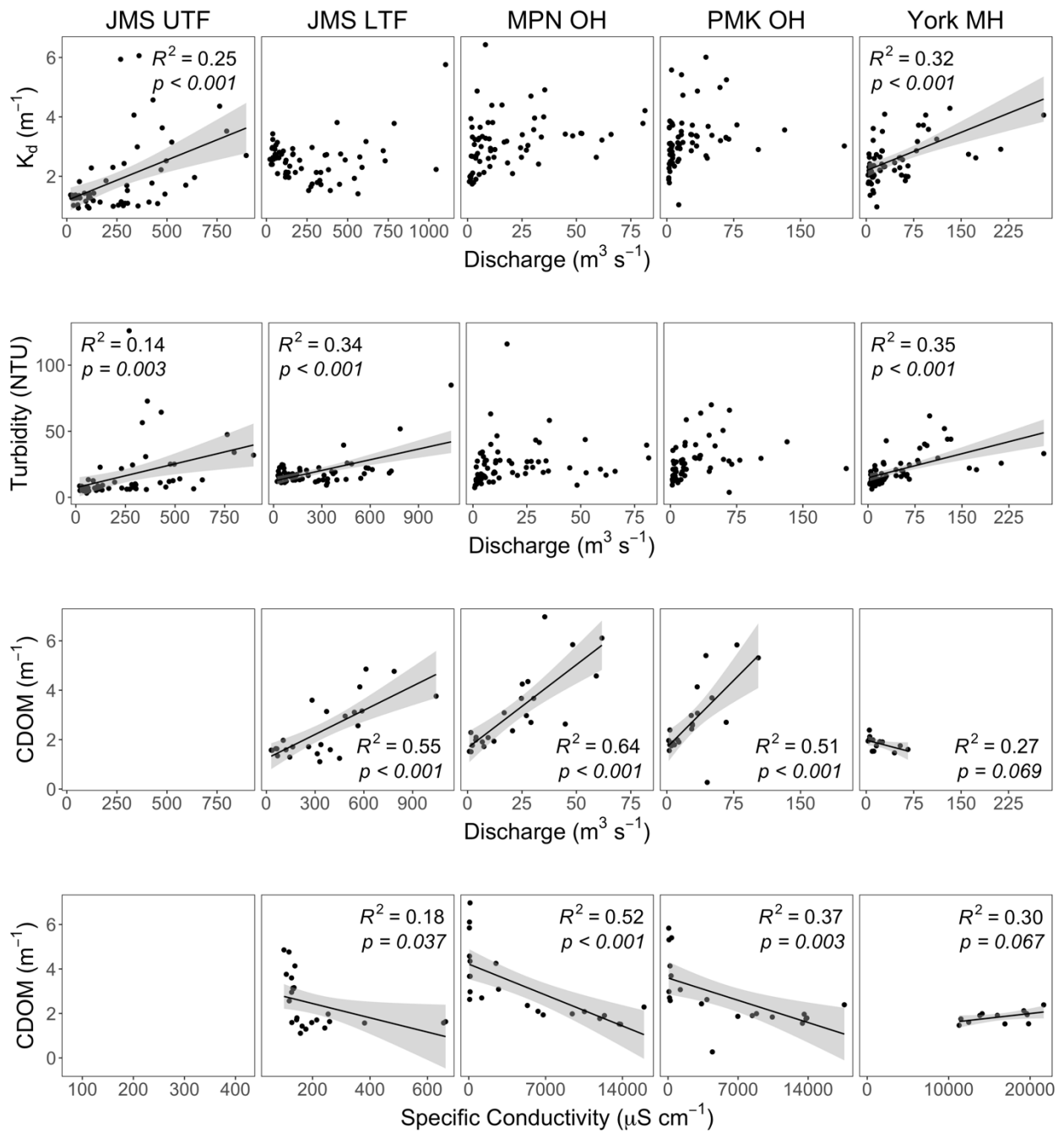
Fig. 9: Linear regressions of K_d, turbidity, and CDOM vs discharge, and CDOM vs conductivity at stations located in the James River upper (JMS UTF) and lower (JMS LTF) tidal fresh segments, Mattaponi (MPN OH) and Pamunkey (PMK OH) oligohaline segments, and the York mesohaline (York MH) segment (no CDOM for JMS UTF). Models with statistically significant ($p < 0.05$) and marginally significant ($0.05 \leq p < 0.10$) results display regression lines. Gray shading represents confidence intervals.

The intercept of the relationship between K_d and turbidity was used as an indicator of light absorption in the absence of scattering (i.e., K_d at turbidity $= 0$). Inferred light attenuation in the absence of scattering ranged from 1.33 (York MH) to 2.22 m^{-1} (MPN OH) and was positively correlated with CDOM (*Fig. 10*).

Fig. 10: Inferred light attenuation in the absence of scattering (K_d at turbidity = 0) in relation to mean CDOM at stations located in the James River lower tidal fresh segment (JMS LTF), Mattaponi (MPN OH) and Pamunkey (PMK OH) oligohaline segments, and the York mesohaline (York MH) segment.
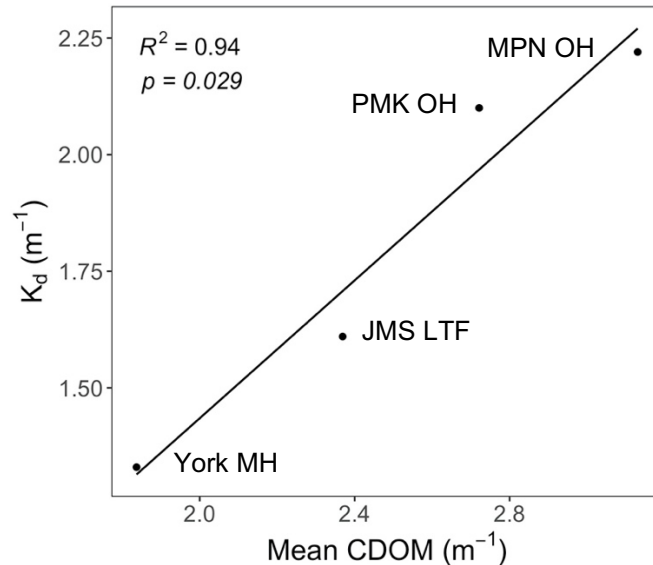
MLR models were derived to quantify contributions from particulate matter (TSS or turbidity, CHLa) and DOM (DOC or CDOM) to K_d. All models containing turbidity performed better than those using TSS. At the JMS UTF, JMS LTF, and the York MH sites, models with the greatest explanatory power included DOC rather than CDOM, while the opposite was true for MPN and PMK OH sites. Top performing MLR models (i.e., models with the greatest R^2; see *Table 1*) accounted for a greater proportion of variation in K_d compared to models based on single predictor variables. Models explained between 64% - 93% of the observed variability in light attenuation among sites with p-values all < 0.001. Comparisons of partial R^2 and p-values from models indicated that turbidity accounted for a significantly greater proportion of variation in K_d than CHLa and DOC or CDOM, alone explaining an average of 67% in total variability.

CHLa was an important factor only at the JMS LTF and York OH sites explaining 33% and 25% in total variability, respectively. At the JMS sites and York MH site, DOC did not account for a significant proportion of variation in K_d (< 4%). At the MPN and PMK OH sites, CDOM was the second most important factor, while CHLa did not hold any predictive power.

Site	R^2	Statistics	Intercept	Turbidity	CHLa	DOC	CDOM
JMS UTF	0.93	coefficient	0.831	0.066	0.002	0.005	
		partial R^2	na	0.92	0.00	0.00	
		p	< 0.001	< 0.001	0.811	0.714	
JMS LTF	0.79	coefficient	1.15	0.053	0.010	0.022	
		partial R^2	na	0.76	0.33	0.04	
		p	< 0.001	< 0.001	< 0.001	0.216	
MPN OH	0.64	coefficient	1.73	0.047	-0.003		0.095
		partial R^2	na	0.48	0.00		0.04
		p	0.004	< 0.001	0.850		0.389
PMK OH	0.64	coefficient	1.66	0.043	-3.9e-4		0.157
		partial R^2	na	0.46	0.00		0.10
		p	0.004	0.001	0.978		0.198
York MH	0.73	coefficient	0.967	0.065	0.019	8.6e-4	
		partial R^2	na	0.72	0.25	0.00	
		p	< 0.001	< 0.001	< 0.001	0.964	

Table 1: Statistics from top performing MLR models at stations located in the James River upper (JMS UTF) and lower (JMS LTF) tidal fresh segments, Mattaponi (MPN OH) and Pamunkey (PMK OH) oligohaline segments, and the York mesohaline (York MH) segment. Coefficient units: intercept = m^{-1}, turbidity = m^{-1} NTU^{-1}, CHLa = m^2 mg^{-1}, DOC = m^2 g^{-1}, CDOM = dimensionless.

Models with the greatest R^2 at each site were used to assess contributions of light attenuating variables to K_d. Turbidity had the greatest contribution to K_d among variables, averaging 1.04 m^{-1} (or 48%) in the JRE and 1.13 m^{-1} (or 40%) in the YRE (*Fig. 11*). The lowest turbidity contributions were at the MPN OH site (1.00 m^{-1}, 33%) and the highest were at the York MH site (1.30 m^{-1}, 51%). CHLa contributions were negligible and inversely related to K_d at MPN and PMK OH sites (-0.032 m^{-1} and -0.005 m^{-1}, or -1.1% and -0.14% respectively). CHLa

contributions to K_d averaged 0.011 to 0.24 m^{-1} (0.56% to 9.6%) in the JRE and -0.032 to 0.28 m^{-1} (-0.14% to 11%) in the YRE. In all models, CHLa had a greater impact in controlling light attenuation during the summer compared to its impact over the entire year. This was especially apparent at the JMS LTF site. DOC contributions to K_d were 0.017, 0.107, and 0.005 m^{-1} (0.90%, 4.2%, and 0.21%) at the JMS UTF, JMS LTF, and York MH sites, respectively. CDOM contributions to K_d were 0.31 m^{-1} (or 10%) at MPN OH and 0.43 m^{-1} (or 14%) at PMK OH. The intercept of the regressions was taken as background attenuation representing water alone plus any other light attenuating matter not characterized by turbidity, CHLa, and CDOM or DOC. Intercepts ranged from 0.83 to 1.73 m^{-1}. The resulting background contributions to light attenuation were between 38% (York MH) and 58% (MPN OH).
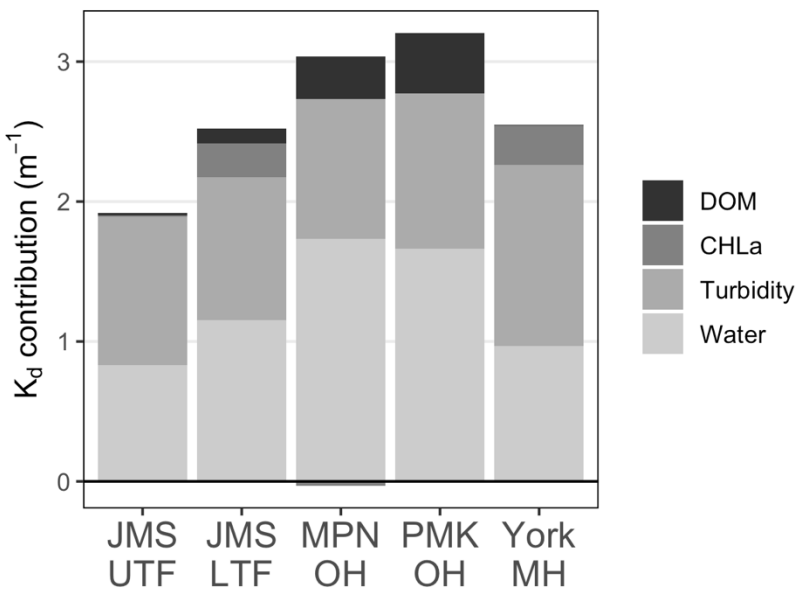
Fig. 11: Contributions from each predictor variable in top performing MLR models (Table 1) at stations located in the James River upper (JMS UTF) and lower (JMS LTF) tidal fresh segments, Mattaponi (MPN OH) and Pamunkey (PMK OH) oligohaline segments, and the York mesohaline (York MH) segment. "DOM" is an abbreviation for dissolved organic matter and represents either DOC (JMS UTF, JMS LTF, York MH) or CDOM (MPN OH, PMK OH). Model intercepts were used to represent water itself and other factors not characterized by predictor variables in each model.

GAMs were derived to identify non-linear trends in light attenuating constituents in each model (*Fig. 12*). Overall, results from the GAMs were relatively similar to MLRs. For all sites, the best model based on MLRs was also the best model as judged by GAMs, except at the MPN OH site in which TSS had greater importance in predicting K_d than turbidity. Comparisons of R^2 values suggest GAM models account for a slightly greater proportion of variation in K_d implying there is non-linearity in the relationships between the independent variables and light attenuation.

Differences were marginal in the James (1% to 2%) and moderately greater in the YRE (8% to 21%).
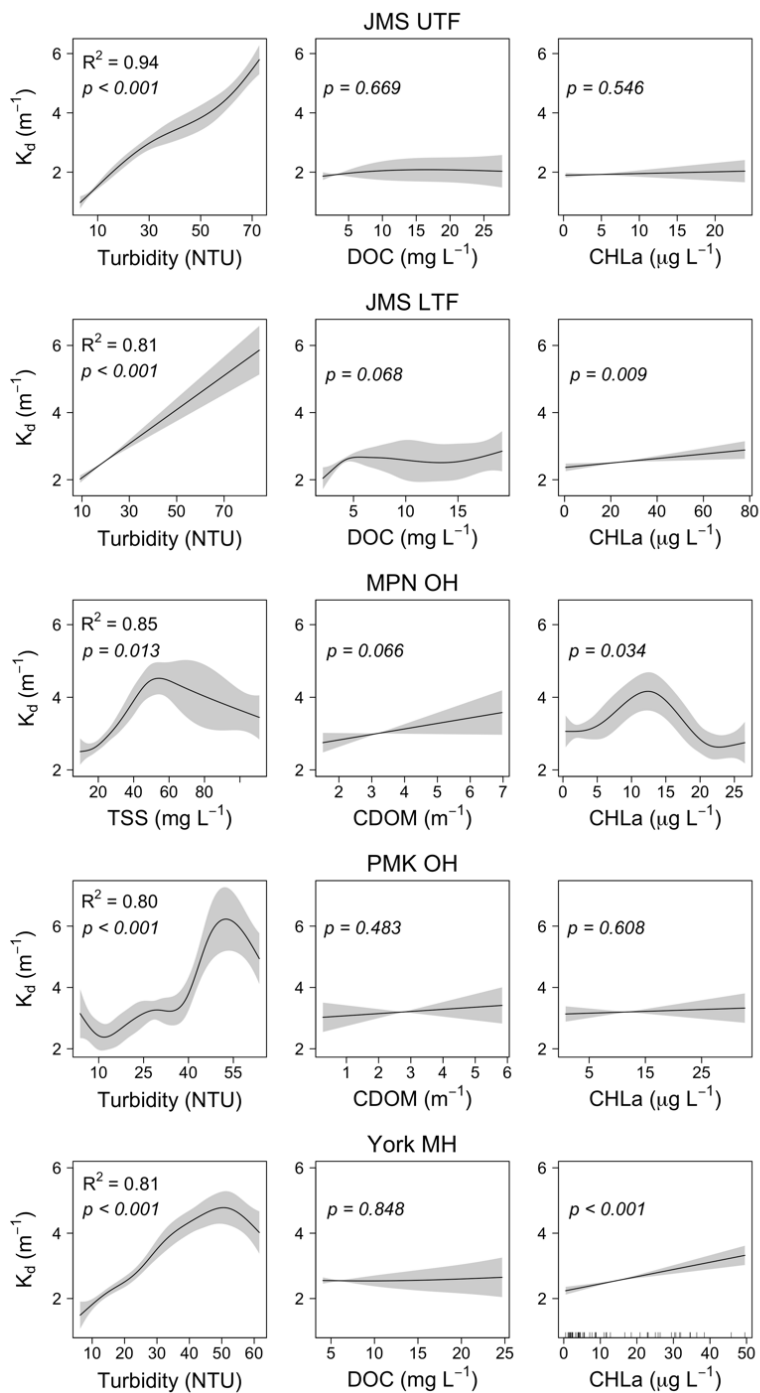
Fig. 12: Results of GAM analysis depicting variation in light attenuation in relation to explanatory variables for stations located in the James River upper (JMS UTF) and lower (JMS LTF) tidal fresh segments, Mattaponi (MPN OH) and Pamunkey (PMK OH) oligohaline segments, and the York mesohaline (York MH) segment. Displayed R^2 is for the overall model. Gray shading represents confidence intervals.

Implications for Primary Producers

Average underwater irradiance (I_{wc}; E m^{-2} day^{-1}) in the James lower TF was used to characterize inter-annual variation in light availability from 2014-2019 (*Fig. 13*; *Table 2*). I_{wc} peaked between late April and early June each year. Means ranged from 3.60 to 5.18 E m^{-2} day^{-1} annually, 5.84 to 7.99 E m^{-2} day^{-1} each spring, and 3.90 to 6.65 E m^{-2} day^{-1} each summer. Coefficients of variation of mean I_{wc} between 2014-2019 were as follows: annual (12.7 %), spring (11.5 %), and summer (17.4 %). Poor light conditions during the summer of 2015 were followed by a drastic decline in SAV coverage in 2016 (228.6 ha to 37.1 ha) despite a significant increase in I_{wc}. Populations then recovered to > 180 ha in 2017. SAV coverage tended to track estimated summer K_d with both exhibiting declines in 2016 and 2018.
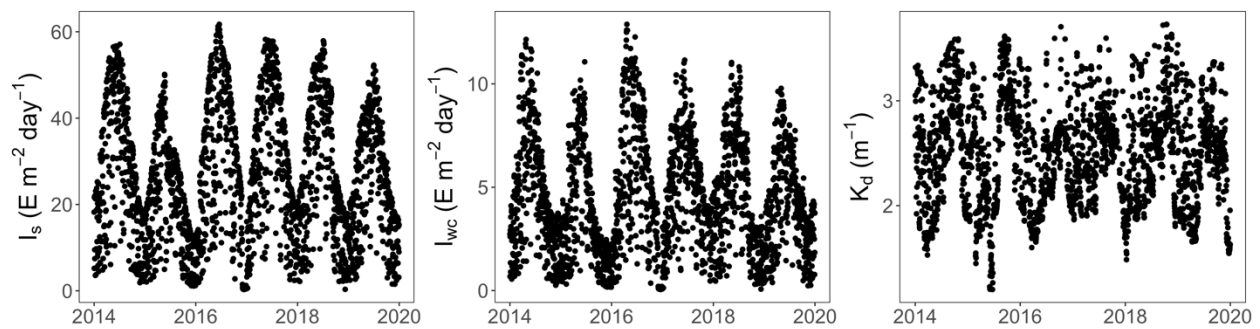
Fig. 13: Average daily incident irradiance (I_s), average daily underwater irradiance (I_{wc}), and GAM predicted K_d in the lower TF segment of the James from 2014-2019.

	Mean total daily I_s		Mean total daily I_{wc}		Predicted K_d		*SAV coverage (ha)
Dataset	Spring	Summer	Spring	Summer	Spring	Summer	JMSTF1
2014	41.09	36.16	7.42	5.25	2.25	2.83	208.2
2015	31.86	24.17	6.44	3.90	2.02	2.70	228.6
2016	39.82	41.20	7.99	6.65	2.02	2.53	37.1
2017	39.28	41.40	6.47	5.91	2.45	2.80	181.5
2018	39.45	36.96	6.48	5.81	2.52	2.61	162.9
2019	32.23	34.28	5.84	5.00	2.29	2.77	214.3
CV	11.0 %	17.7 %	11.5 %	17.4 %	9.4 %	4.3 %	40.8 %

Table 2: Average daily incident irradiance (I_s), underwater irradiance (I_{wc}), and GAM predicted K_d in the James lower TF segment from 2014-2019 during spring and summer seasons. CVs are the coefficients of variation between 2014-2019 means.
*SAV coverage data (hectares) in the James lower tidal fresh (JMSTF1) collected by the Virginia Institute of Marine Sciences (VIMS)

A previous study on U.S. Midwest rivers by Koch et al. (2004) suggests that phytoplankton are light limited when underwater irradiance is < 5 E m^{-2} day^{-1}. Given that the other major constraint is freshwater residence time (FRT= 28 days), we analyzed the yearly distribution of discharge versus I_{wc} from 2014-2019 in the James lower TF during the warm weather season (April-October) when temperature is less likely to limit phytoplankton. Data was indexed to distinguish periods when discharge and light availability may have been constraining to phytoplankton growth (*Fig. 14*). The percentage of days having both favorable light and discharge conditions ($I_{wc} > 5$ E m^{-2} day^{-1}, discharge < 100 m^3 s^{-1}) ranged from 10% (2018) to 35% (2017) with a CV of 56.2%. Favorable conditions were more frequent in the years 2014, 2016, and 2017 (> 20%) compared to other years (< 11%).
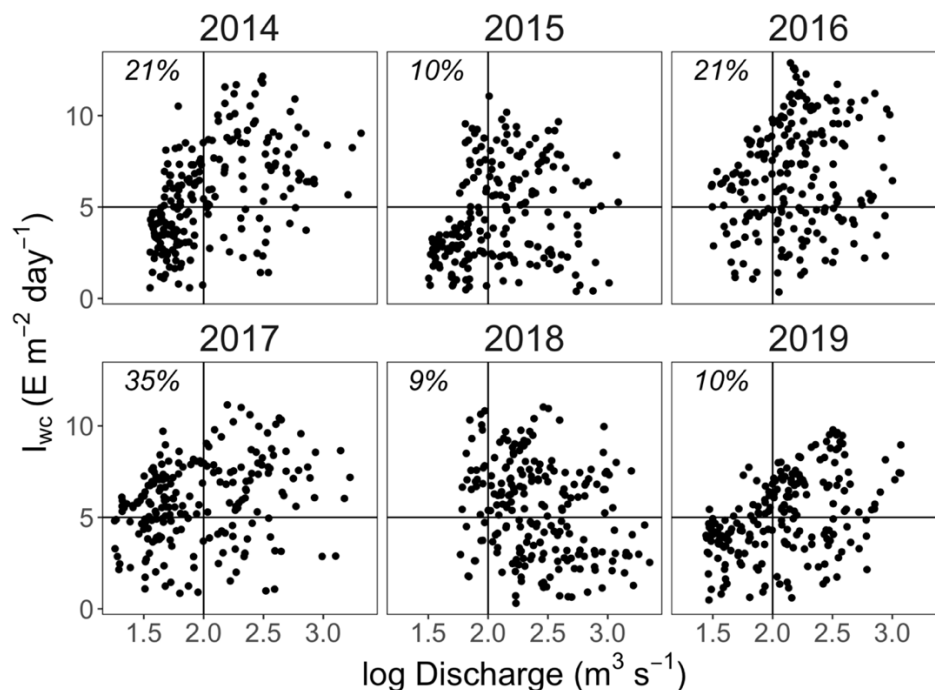
Fig. 14: Log of average daily discharge vs average daily underwater irradiance (I_{wc}) in the James lower TF from 2014-2019 during the warm season (April-October). Horizontal lines (y = 5 E m^{-2} day^{-1}) delineate the threshold for light-limiting conditions, and vertical lines (x = log(100 m^3 s^{-1})) distinguish the threshold for hydrologic-limiting conditions. Percentages displayed in plots are the number of days per year considered to have both favorable light and discharge conditions (upper, left quadrant).

Discussion

This study describes the impacts of optically active constituents (i.e., CHLa, TSS, DOM) on the diffuse light attenuation coefficient (K_d) in the upper segments of two estuaries. Since both estuaries are river dominated, we intended to assess the extent of light attenuation regulated by internal processes (phytoplankton) versus external inputs (non-living suspended solids and DOM). Results indicated that in both estuaries, turbidity had the greatest impact on water clarity. Internal processes did not dominate variations in light attenuation as CHLa was not a significant predictor of K_d at any site. This also suggests that algae comprised only a small proportion of the measured suspended particulate matter. Strong correlations between turbidity and TSS, and weak

26

correlations between turbidity and CHLa also indicate most of the measured suspended particulate matter was non-algal (e.g., silt and clay).

Regressions between turbidity and TSS revealed that the JRE had almost double the amount of light scattering per unit mass of suspended solid compared to the YRE. In general, the amount of light scattering by suspended solids is dependent on particle composition, with finer particles having a greater negative impact on water clarity. Analysis of particle size data did not reveal significant differences in particle diameter or mass between JRE sites and YRE sites. Therefore, we could not attribute the higher amount of light scattering per unit mass observed in the JRE to differences in particle size. While we would expect to see a strong relationship between turbidity and particle density at all study sites, comparisons of regression R^2 values showed significantly higher correlations at MPN and PMK OH sites compared to JMS sites. One explanation for this is that the Coulter counter used to measure particle data had a minimum operational range of 2 μm meaning it was not able to analyze particles below this size. It is possible there were suspended particles below 2 μm present at sites (specifically JMS sites) that were not accounted for in the data. To test this possibility, water samples collected from JMS sites were run separately through a 1 μm and 2 μm filter. The 1 μm filter collected 12% and 49% more sediment than the 2 μm filter at the JMS LTF and JMS UTF sites, respectively, indicating there may have been particles < 2 μm present. This suggests Coulter counter data may be under-estimating particle density at these sites by 10-50%. If true, this would affect the estimation of particle mass (particle density/TSS) since particle density data encompassed particles > 2 μm, whereas TSS filters captured particles > 0.5 μm. Additionally, if the JMS sites had a greater proportion of fine particles compared to the YRE sites, this may also help explain the greater amount of light scattering per unit mass at the JMS sites.

While non-living suspended solids were the strongest predictors of variation in light attenuation, results indicate CDOM also had a significant impact at the JMS LTF, MPN OH, and PMK OH sites. This suggests external inputs deliver considerable amounts of DOM to these water columns which negatively impact water clarity. Although CDOM absorbs light, it does not contribute significantly to scattering (Kirk 1994). When the effects of scattering were removed (i.e., K_d at turbidity = 0), increases in CDOM correlated with increases in K_d indicating CDOM

may be an important parameter impacting background clarity. At the JMS LTF, MPN OH, and PMK OH sites, CDOM concentrations were positively correlated with discharge, however, a similar negative correlation was observed between CDOM and specific conductivity. USGS discharge used in the analysis was measured well upstream from our sampling locations and as a result may not be reflective of freshwater influences arising from local runoff. Therefore, we suspect conductivity could be used as a surrogate to assess freshwater influences. In this case, the inverse relationship between CDOM and conductivity implies that CDOM inputs decline with declining freshwater inputs.

Empirical models derived from in situ observations of K_d, CHLa, turbidity, and DOC or CDOM allowed us to assess the impact of varying light attenuating constituents to K_d. Since linear regressions indicated turbidity correlated well with TSS but not CHLa, turbidity was used only to represent non-living suspended solids. And since the CDOM dataset was limited (less than half that of DOC), CDOM and DOC were used interchangeably to represent DOM. While previous studies have reported significant correlations between CDOM and DOC (Vodacek et al. 1995; Ferrari et al. 1996; Ferrari 2000; Rochelle-Newall and Fisher 2002), our statistical regressions showed a weak correlation ($R^2 < 0.17$ for all sites), meaning DOC during the sampling period may not accurately reflect the fraction of DOM contributing to light attenuation. However, MLR models using DOC data limited to the CDOM same sampling period returned similar K_d predictions with comparable predictive power (not shown here). This suggests DOC may be a suitable surrogate for CDOM in our predictive models. Since CDOM and conductivity tended to have a good correlation, we also tried using conductivity as a substitute for CDOM, but this did not improve model performance. Using derived MLR models, the attenuation of water alone (regression intercept) was found to be between 0.83 and 1.73 m^{-1}. In a study on the Chesapeake Bay and its tidal tributaries, Gallegos and Moore (2000) reported the specific attenuation coefficients for water alone as ranging from 0.4 to 3.2 m^{-1}. They considered these values high and did not believe they were representative of the actual attenuation of water itself with all other optical components removed. They suggest rather that the regression is lumping all unexplained variance into one intercept. In the same study they reported specific attenuation coefficients for DOC ranging from 0.026 m^2 g^{-1} in TF areas to 0.031 m^2 g^{-1} in MH conditions. Although none of our coefficients representing DOM were statistically significant, DOC values

at the JMS LTF site ($0.022 \ m^2 \ g^{-1}$) compare favorably with those reported by Gallegos and Moore (2000). DOC at the JMS UTF and York MH site contributed significantly less, while CDOM coefficients were considerably higher. Our turbidity coefficients were low compared to the TSS coefficient used in the final Gallegos and Moore (2000) model ($0.094 \ m^2 \ g^{-1}$), but aligned well with a model by Xu et al (2005) who reported a TSS coefficient of $0.059 \ m^2 \ g^{-1}$ for the Chesapeake Bay. The CHLa coefficient used in the final Gallegos and Moore (2000) model ($0.016 \ m^2 \ mg^{-1}$) was similar only to our CHLa coefficient at the JMS LTF ($0.010 \ m^2 \ mg^{-1}$) and York MH ($0.019 \ m^2 \ mg^{-1}$) sites. Although insignificant ($p > 0.05$), the negative coefficients for CHLa at the MPN and PMK OH are somewhat conflicting given that increases in phytoplankton biomass should lead to greater light attenuation. Negative CHLa coefficients derived in the model by Gallegos and Moore (2000) were considered to be ambiguous, however, Xu et al (2005) suspected the results were reflective of light limitation on phytoplankton growth. In clearer water (lower K_d) with less suspended sediments, CHLa may strongly influence K_d creating a positive correlation. However, in turbid water with low water clarity (higher K_d), CHLa concentrations may be low because light is limiting phytoplankton photosynthesis. Therefore, an inverse relationship between K_d and CHLa exists. We suspect the inverse relationship between K_d and CHLa, can also be explained by increases in discharge. Water clarity in the YRE is controlled by external inputs (TSS and CDOM) which typically increase with discharge, whereas CHLa tends to decrease. Therefore, increases in discharge can lead to increases in K_d, while simultaneously decreasing CHLa. Although a strong relationship between discharge and TSS and discharge and CDOM were not observed in this study, regressions between discharge and CHLa at the MPN and PMK OH showed a moderately negative relationship (data not shown; $R^2 = 0.27$ and 0.21, respectively).

Previous research has supported the use of nonparametric GAM methods in water quality data analysis (Richards et al. 2013, Morton and Henderson 2008). In GAM models, relationships between independent and dependent variable are not assumed to be linear, allowing for flexible predictor functions to uncover hidden patterns in data. This can be especially useful when analyzing seasonal trends in water quality. For instance, a timeseries of our observed K_d values did not reveal any obvious seasonal trends. However, GAMs using long-term CBP K_d data with day of year as a predictor variable identified seasonal declines in late summer (Pamunkey and

York sites) and early spring (James lower TF). We also used GAMs to identify non-linear trends in light attenuating constituents (suspended solids and DOM). Although GAM results suggested there was some nonlinearity present in the data, relationships between K_d and predictor variables appeared fairly linear. This supported the use of our MLR models which, unlike GAMs, provided specific attenuation coefficients that allowed us to quantify individual contributions of each predictor variable to K_d.

The relatively small contribution of CHLa and DOM to light attenuation as compared to turbidity has important management implications. For example, considerable reductions in CHLa may not significantly increase water clarity if K_d is controlled largely by suspended sediments. Rather than focusing on nutrient reductions to limit phytoplankton biomass, emphasis may need to be placed on strategies aimed at limiting activities leading to increased sediment inputs (e.g., dredging and erosion). That said, nutrient load reductions in eutrophic waterbodies have been shown to significantly improve water clarity. This was demonstrated in a recent study by Jones (2018) on a shallow (mean depth = 1.5 m) TF embayment of the Potomac River (Gunston Cove in Fairfax County, Virginia), another main tributary to the Chesapeake Bay. SAV populations in this area experienced drastic declines until they nearly disappeared due to eutrophication. Major reductions in phosphorous point source inputs (95%), lead to decreases in CHLa concentrations from > 80 to 20 $\mu g\ L^{-1}$ and improved water clarity from 3.7 to 2.0 m^{-1}. Additionally, SAV populations recolonized > 200 ha of shallow area in the embayment. The James River TF region has also experienced large reductions in point source nutrient inputs (Bukaveckas and Isenberg 2013), but without accompanied declines in CHLa concentrations. Over a 25-year span (1985-2010), nitrogen point source loads were reduced by 50% and phosphorous point source loads were reduced by 73%. From 1998 to 2005 SAV coverage remained below 40 ha in the James lower TF, however, coverage began steadily increasing in 2006 and reached 214 ha in 2019. SAV coverage in the James upper TF remains low in comparison (< 5 ha). CBP long-term data showed water clarity has steadily improved from a mean K_d value of 3.4 m^{-1} between 1994-1999 to 2.9 m^{-1} in the past 5 years. However, improvement in water clarity and proportional SAV coverage in the James is marginal compared to that seen at Gunston Cove. This is surprising considering increases in water clarity should have a greater positive impact in deeper water due to the exponential decline of light with depth. Despite high algal populations in the James lower

30

TF, our results indicate that management activities aimed at controlling suspended solids should have a more positive impact on water clarity than reductions in nutrient inputs. However, increases in rooted SAV species should theoretically control suspended solid concentrations by limiting shoreline erosion. Although this may be attributed to management activities other than SAV recovery, CBP data show TSS declined from a mean value of 30.1 mg L^{-1} in the late 1990s to 20.3 mg L^{-1} in recent years. Gunston Cove saw reductions from 23 to 15 mg L^{-1}. This not only demonstrates the important balance between factors affecting water clarity within these systems, but also suggests that over time nutrient reductions in eutrophic waterbodies could help manage high TSS concentrations. Although we would have expected to see greater increases in SAV coverage with past reductions in TSS, it is possible that the majority of the James lower TF is too deep to support large populations of SAV.

Although there is an abundance of literature about the relationships between light availability and SAV distribution in freshwater lakes and PH environments, there is relatively less information in TF, OH and MH estuarine environments (Batiuk et al. 2000). These environments are often characterized by high turbidity, tidal fluctuations, variable salinity and high-energy events (i.e., wind and waves). In general, there is a strong positive relationship between water clarity and the maximum water-column depth to which SAV species grow. The maximum depth of colonization is greater for TF and OH species, implying a higher percent of surface light reaching SAV habitat is necessary for the growth and survival of MH and PH species (Vant et al. 1986; Dennison 1987). The minimum recommended light requirement for SAV growth and survival at a 1 m depth in the Chesapeake Bay and its tidal tributaries is a $K_d \leq$ 2.0 (13% of surface irradiance) in TF and OH areas and a $K_d \leq 1.5$ (22% of surface irradiance) in MH and PH areas (Batiuk et al. 2000). Using the below equation, we determined the percent of surface light reaching a 1 m depth at each site for comparison against light availability recommendations.

% light = 100*exp(-K_d*1 m)

During our study period, the JMS UTF (25.54%) site was the only habitat that could have supported the growth of SAV at a 1 m depth. All other sites failed to meet recommended light

requirements (JMS LTF = 7.8%, MPN OH = 4.5%, PMK OH = 4.4%, York MH = 9.5%). Comparisons between MPN and PMK OH sites indicate slight differences in median K_d values (3.11 m^{-1} and 3.13 m^{-1}, respectively) result in similar percent light availability at any given depth. When K_d is decreased by about half (1.37 m^{-1}; JMS UTF), light availability is 240% greater at a depth of 0.5 m and over 500% greater at a depth of 1 m. Therefore, a higher K_d is more detrimental to SAV at greater depths compared to more shallow depths.

To further assess SAV light availability, we evaluated the inter-annual variation in underwater light irradiance in the James lower TF. Average daily underwater irradiance (I_{wc}) was estimated using K_d values predicted by a GAM model derived using, turbidity, day of year, and decimal date as predictor variables. The coefficient of variation of mean I_{wc} values did not show a significant change in underwater light availability between 2014-2019 (< 25 %). This implies light conditions were relatively similar from year to year. The same was true for spring and summer seasons. Increases in underwater light availability are expected to increase SAV growth due to more favorable light conditions. A decline in I_{wc} in 2015 preceded a large drop-off in SAV in the James lower TF in 2016. This suggests that despite statistical similarities in underwater irradiance, patterns in SAV growth may have responded to variations in light availability but with a lag period of one year. However, SAV populations seemed to better track predicted summer K_d as slight declines in mean K_d in 2016 and 2018 corresponded to declines in SAV coverage. This indicates SAV growth is more directly impacted by water clarity than underwater irradiance. Average daily I_{wc} and discharge data was analyzed to determine the percentage of days having both favorable light and water residence time conditions (I_{wc} > 5 E m^{-2} day^{-1}; discharge < 100 m^3 s^{-1}). The CV of percentages from 2014-2019 was 56.17% suggesting there was significant variation in favorable conditions from year to year. Surprisingly, this did not appear to have any significant correlation with SAV coverage or algal abundance. For instance, despite a considerable increase in the percentage of days with favorable conditions from 2015 to 2016 (10.4% to 20.6%), SAV coverage decreased drastically from 228.6 to 37.1 ha. Perhaps, favorably light conditions allowed for increased phytoplankton growth which attenuated light reaching SAV beds.

Conclusion

We have demonstrated how statistical methods using water quality data from discrete monitoring can be used to assess impacts of light attenuating constituents on K_d. Despite differences in characteristics among study sites, findings suggest that turbidity was the strongest predictor of light attenuation variation in all three sub-estuaries studied. This has important implications on how these habitats should be managed. For instance, management strategies focused on improving water clarity should target anthropogenic impacts that cause increases in suspended sediment loads (e.g., dredging, erosion, and land use changes)

Confounding results from our statistical models (i.e., negative attenuation coefficients, large attenuation coefficients for water alone, lack of significant light attenuating variables) demonstrated how optically complex and variable these environments are, making it difficult to estimate influences of various factors on water clarity. Another challenge we faced was the presence of competing variables. In turbid water light is typically a limiting factor in phytoplankton growth, whereas in clearer water other factors such as nutrients may be the limiting factor. We suspect that this resulted in negative correlations between CHLa and K_d despite the light attenuating properties of CHLa. Competition between light attenuation by phytoplankton and light control of phytoplankton growth in turbid water may also have led to an underestimation of the net contribution of phytoplankton to light attenuation. GAMs proved to be a valuable supplement to our water quality analyses as they provide a more flexible interpretation of data. GAM models were especially useful in uncovering hidden seasonal patterns in K_d.

We also show how continuous monitoring data can be incorporated into statistical models used to predict light attenuation over periods in which there were gaps in K_d data. In this case, continuous datasets can be used to better resolve seasonal and inter-annual variability in light conditions. This may lead to a better understanding of how light conditions affect algal blooms and the success of SAV restoration.

Information gathered from light attenuation studies is instrumental in determining the appropriate management strategies aimed at improving poor water conditions. We hope findings

presented here provide a better understanding of factors regulating light attenuation in the upper estuary and help aid in management decisions aimed at restoring estuarine water clarity.

References

Abdelrhman, M.A. 2017. Quantifying Contributions to Light Attenuation in Estuaries and Coastal Embayments: Application to Narragansett Bay, Rhode Island. *Estuaries and Coasts* 40: 994-1012.

Baldizar, J.M., and N.B. Rybicki. 2006. Primary factors affecting water clarity at shallow water sites throughout the Chesapeake and Maryland coastal bays. *Proceedings of the Eighth Federal Interagency Sedimentation Conference* 1027-1034.

Batiuk, R.A., P. Bergstrom, M. Kemp, E. Koch, L. Murray, J. Court Stevenson, R. Bartleson, et al. 2000. Chesapeake Bay submerged aquatic vegetation water quality and habitat-based requirements and restoration targets: A second technical thesis. Annapolis, MD, USA: Chesapeake Bay Program; EPA.

Bukaveckas, P.A., L.E. Barry, M.J. Beckwith, V. David, and B. Lederer. 2011. Factors determining the location of chlorophyll maximum and the fate of algal production within the tidal freshwater James River. *Estuaries and* Coasts 34 (3): 569-582.

Bukaveckas, P.A., and W.N. Isenberg. 2013. Loading, transformation, and retention of nitrogen and phosphorus in the tidal freshwater James River (Virginia). *Estuaries and Coasts* 36 (6): 1219-1236.

Bukaveckas, P.A., M. Beck, D. Devore, and W.M. Lee. 2018. Climatic variability and its role in regulating C, N and P retention in the James River Estuary. *Estuarine, Coast and Shelf Science* 205: 161-173.

Bukaveckas, P.A, M. Katarzyte, A. Schlegel, R. Spuriene, T Egerton, and D. Vaiciute. 2019. Composition and settling properties of suspended particulate matter in estuaries of the Chesapeake Bay and Baltic Sea regions. *Journal of Soil and Sediments* 19: 2580-2593.

Chen, Z.C., and P.H. Doering. 2016. Variation of light attenuation and the relative contribution of water quality constituents in the Caloosahatchee River Estuary. *Florida Scientist* 79 (2-3): 93-108.

Davies-Colley, R.J., and D.G. Smith. 2001. Turbidity, suspended sediment, and water clarity: a review. *Journal of the American Water Resources Association* 37 (5): 1085-1101.

Davies-Colley, R.J., D.J. Ballant, S.H. Elliot, A. Swales, A.O. Hughes, and M.P. Gall. 2014. Light attenuation – a more effective basis for the management of fine suspended sediment than mass concentration?. *Water Science & Technology* 69: 1867-1874.

Dennison, W.C. 1987. Effects of light on seagrass photosynthesis, growth and depth distribution. *Aquatic Botany* 27(1):15-26.

Dennison, W.C., R.J. Orth, J.C. Stevenson, V. Carter, S. Kollar, P.W. Bergstrom, and R.A. Batiuk. 1993. Assessing water quality with submersed aquatic vegetation. *BioScience* 43 (2): 86-94.

Ferrari, G.M., M.D. Dowell, S. Grossi, and C. Targa. 1996. Relationship between the optical properties of chromophoric dissolved organic matter and total concentration of dissolved organic carbon in the southern Baltic region. *Marine Chemistry* 55 (3): 299-316.

Ferrari, G. M. 2000. The relationship between chromophoric dissolved organic matter and dissolved organic carbon in the European Atlantic coastal area and in the West Mediterranean Sea (Gulf of Lions). *Marine Chemistry* 70 (4): 339-357.

Gallegos, C.L. 1994. Refining habitat requirements of submersed aquatic vegetation: role of optical models. *Estuaries* 17 (1):198-219.

Gallegos, C.L., and K.A. Moore. 2000. Factors contributing to water-column light attenuation. In Chesapeake Bay submerged aquatic vegetation water quality and habitat-based requirements and restoration targets: a second technical synthesis, by R.A. Batiuk, 35-54. Annapolis, MD: EPA Chesapeake Bay Program.

Gallegos, C.L. 2001. Calculating optical water quality targets to restore and project submersed aquatic vegetation: Overcoming problems in partitioning the diffuse attenuation coefficient for photosynthetically active radiation. *Estuaries* 24 (3): 381-397.

Gallegos, C.L., T.E. Jordan, A.H. Hines, and D.E. Weller. 2005. Temporal variability of optical properties in a shallow, eutrophic estuary: seasonal and interannual variability. *Estuarine, Coastal, and Shelf Science* 64 (2-3): 156-170.

Gosselain, V., J.P. Descy, and E. Everbecq. 1994. The phytoplankton community of the River Meuse, Belgium: Seasonal dynamics (year 1992) and the possible incidence of zooplankton grazing. *Hydrobiologia* 289 (1): 179-191.

Haas, L.W. 1977. The effect of the spring-neap tidal cycle on the vertical salinity structure of the James, York, and Rappahannock Rivers, Virginia, USA. *Estuaries and Coasts* 5 (4): 485-496.

Haas, L.W., S.J. Hastings, and K.L. Webb. 1981. Phytoplankton response to a stratification-mixing cycle in the York River estuary during late summer. In Estuaries and Nutrients, by B.J. Neilson and L.E. Cronin. Clifton, NJ: Humana Press.

Hayward, D., C.S. Welch, and L.W. Haas. 1982. York River destratification: an estuary-subestuary interaction. *Science* 216 (4553):1413-1414.

Jones, R.C. 2020. Recovery of a Tidal freshwater embayment from eutrophication: a multidecadal study. *Estuaries and Coasts* 43 (2): 1318-1334.

Kemp, W.M., W.R. Boynton, J.E. Adolf, D.F. Boesch, W.C. Boicourt, G. Brush, J.C. Cornwell, T.R. Fisher, P.M. Glibert, J.D. Hagy, L.W. Harding, E.D. Houde, D.G. Kimmel, W.D. Miller, R.I.E. Newell, M.R. Roman, E.M. Smith, and J.C. Stevenson. 2005. Eutrophication of Chesapeake Bay: Historical trends and ecological interactions. *Marine Ecology Progress Series* 303: 1-29.

Kirk, J.T.O. 1994. Photosynthesis in aquatic ecosystems, 2nd ed. New York, NY: Cambridge University Press.

Kirk, J.T.O. 2011. Light and Photosynthesis in aquatic ecosystems, 3rd ed. New York, NY: Cambridge University Press.

Koch, R.W., D.L. Guelda, and P.A. Bukaveckas. 2004. Phytoplankton growth in the Ohio, Cumberland and Tennessee Rivers, USA: inter-site differences in light and nutrient limitation. *Aquatic Ecology* 38 (1): 17-26.

Lake, S.J., M.J. Brush, I.C. Anderson, and H.I. Kator. 2013. Internal versus external drivers of periodic hypoxia in a coastal plain tributary estuary: the York River, Virginia. *Marine Ecology Progress Series* 492: 21-39.

Morton, R., and B.L. Henderson. 2008. Estimation of nonlinear trends in water quality: An improved approach using generalized additive models. *Water Resources Research* 44 (7): W07420.

Qin, Q., and J. Shen. 2017. The contribution of local and transport processes to phytoplankton biomass variability over different time scales in the Upper James River, Virginia. *Estuaries and Coasts* 196: 123-249.

Reay, W.G. 2009. Water quality within the York River. *Journal of Coastal Research* 57: 23-39. Richards, R., L. Hughes, D. Gee, and R. Tomlinson. 2013. Using generalized additive models for water quality assessments: A case study example from Australia. *Journal of Coastal Research* 65: 111-116.

Richards, R., L. Hughes, D. Gee, and R. Tomlinson. 2013. Using generalized additive models for water quality assessments: A case study example from Australia. *Journal of Coastal Research* 65: 111-116

Rochelle-Newall, E.J., and T.R. Fisher. 2002. Chromophoric dissolved organic matter and dissolved organic carbon in Chesapeake Bay. *Marine Chemistry* 77 (1): 23-41.

Smock, L.A., A.B. Wright, and A.C. Benke. 2005. Atlantic Coast Rivers of the southeastern United States. In Rivers of North America, by A.C. Benke and C.E. Cushing, 73-122. New York, NY: Elsevier.

Tassone, S.J., and P.A. Bukaveckas. 2019. Seasonal, interannual, and longitudinal patterns in estuarine metabolism derived from diel oxygen data using multiple computational approaches. *Estuaries and Coasts* 42 (1): 1032-1051.

Vant, W.N., R.J. Davies-Colley, J.S. Clayton, and B.T. Coffey. 1986. Macrophyte depth limits in North Island (New Zealand) lakes of differing clarity. *Hydrobiologia* 137 (1): 55-60.

Vodacek, A., F.E. Hoge, R.N. Swift , J.K. Yungel, E.T. Peltzer, and N.V. Blough. 1995. The use of in situ and airborne fluorescence measurements to determine UV absorption coefficients and DOC concentrations in surface waters. *Limnology and Oceanography Letters* 40 (2): 411-415.

Wood, J.D., and P.A. Bukaveckas. 2014. Increasing severity of phytoplankton nutrient limitation following reductions in point source inputs to the tidal freshwater segment of the James River Estuary. *Estuaries and Coasts* 37 (5): 1188-1201.

Wood, J.D., D. Elliot, G. Garman, D. Hopler, W.M. Lee, S. McIninch, A.J. Porter, and P.A. Buckaveckas. 2016. Autochthony, allochthony and the role of consumers in influencing the sensitivity of aquatic systems to nutrient enrichment. *Food Webs* 7: 1-12.

Xu, J., R.R. Hood, and S.Y. Chao. 2005. A simple empirical optical model for simulating light attenuation variability in a partially mixed estuary. *Estuaries and Coasts* 28 (4): 572-580.